



ORIGINAL ARTICLE

Polymer functionalization of biochar-based heterogeneous catalyst with acid-base bifunctional catalytic activity for conversion of the insect lipid into biodiesel



Weiliang Feng^{a,c}, Xinlong Tie^a, Xiaoling Duan^{b,*}, Su Yan^a, Si Fang^a,
Tielin Wang^{a,c,*}, Peiyong Sun^d, Lin Gan^e

^a School of Chemical Engineering and Pharmacy, Wuhan Institute of Technology, Wuhan 430073, China

^b Hubei Key Laboratory of Purification and Application of Plant Anti-Cancer Active Ingredients, Hubei University of Education, Wuhan 430205, China

^c Key Laboratory of Novel Reactor and Green Chemical Technology of Hubei Province, Wuhan Institute of Technology, Wuhan 430073, China

^d Beijing Key Laboratory of Enze Biomass Fine Chemicals, Beijing Institute of Petrochemical Technology, Beijing 102617, China

^e Chongqing Key Laboratory of Soft-Matter Material Chemistry and Function Manufacturing, School of Chemistry and Chemical Engineering, Southwest University, Chongqing 400715, China

Received 3 December 2022; accepted 13 March 2023

Available online 18 March 2023

KEYWORDS

Polymer meditation;
Insect lipid;
Bifunctional catalyst;
Synergistic effect;
Biodiesel

Abstract This paper focused on the utilization of the waste insect shell for the development of a novel biochar-based heterogeneous catalyst (ZnO/PVP_{mediate}-BC-S) with a highly acid-base bifunctional catalytic capacity for the conversion of the insect lipid into biodiesel. The introduction of polyvinyl pyrrolidone (PVP) as a support mediator was believed to improve the textural properties of support and catalytic activity of the catalyst for the conversion reaction. Meanwhile, the physicochemical properties of the synthesized composite catalyst were characterized with XRD, SEM, TEM, XPS, BET, and FT-IR analysis. The high biodiesel yield (94.36%) was obtained at the defined condition (carbonization temperature = 600 °C, Zn(Ac)₂ concentration = 0.3 mol/L, PVP amount = 35 wt%, reaction temperature = 65 °C, catalyst loading = 6 wt%, methanol/lipid molar ratio = 9:1). Moreover, the possible catalytic mechanism of the prepared catalyst was

* Corresponding authors at: School of Chemical Engineering and Pharmacy, Wuhan Institute of Technology, Wuhan 430073, China (T. Wang).
E-mail addresses: 523043604@qq.com (X. Duan), witwangtl@hotmail.com (T. Wang).

Peer review under responsibility of King Saud University.



comprehensively described. In addition, the stability and reusability of the prepared catalyst during five reaction cycles were also demonstrated. Finally, the physicochemical properties of the biodiesel studied were well comparable with the ASTM standard as well as with the reported literature.

© 2023 The Authors. Published by Elsevier B.V. on behalf of King Saud University. This is an open access article under the CC BY-NC-ND license (<http://creativecommons.org/licenses/by-nc-nd/4.0/>).

1. Introduction

Due to the increasing urgent concern about energy scarcity and environmental pollution, the use of alternatives to traditional fossil fuels has drawn increasingly attractive in recent years (Liang et al., 2022; Cipolletta et al., 2022). Biodiesel, as a sustainable, biodegradable, and clean fuel, can be produced from conventional lipid feedstocks (Ennaceri et al., 2022; Costa and Oliveira, 2022).

Hermetia illucens L. is a non-pest, which is found in warm temperate regions worldwide (Rehman et al., 2017). Commonly, insect larvae can feed on various kinds of organic matter in the biowastes (Lalander et al., 2019). Importantly, insect larvae have high levels of lipids after decomposing this organic waste (Deng et al., 2022). The sum of saturated and unsaturated fatty acids accounted for more than 90% of the total insect lipids. In recent years, the city of Wuhan in China has been producing roughly 365,000 tons of kitchen waste annually (Zheng et al., 2012). Meanwhile, approximately 3,000 tons of insect lipids will be produced. Due to society's environmental awareness and the considerably high production of insect lipids, the energy insect larvae as a renewable resource are expected to have great potential for biodiesel production (Li et al., 2015; Feng et al., 2019).

Many investigations have been reported on biodiesel production by using solid sulfonated carbon-based biomass catalysts (Mansir et al., 2017; Ibrahim et al., 2020). Recently, various biomass wastes have been converted into sulfonated carbon supports for biodiesel production. In this study, in continuation of our interest in the development of renewable methodologies, the waste biomass carbon was derived from the shell of the energy insect (*Hermetia illucens L.*) as above. The life cycle of the insect consists of four stages: egg, larva, pupa, and adult (Proc et al., 2020). The process of pupation is the transformation from a pupa into a fly. The adult fly will crawl out from the part of the shell and then fly away (Raksasat et al., 2020). This process is similar to the cocooning process of butterflies. A large number of insect shells as residues were generated during pupation. Notably, the insect shell has a unique composition (called chitin) and can be used as a bio-waste carbon feedstock with cost-free and renewable (Guo et al., 2021). The utilization of the energy insect shell as a good candidate feedstock is expected to be highly promising for synthesizing sulfonated activated biochar.

In addition, it should be noted that the metal oxide elements as promoters have been introduced into sulfonated carbon-based biomass catalysts to induce and accelerate the conversion of oils. Among these, zinc oxide (ZnO) is extensively used as a solid base catalyst because of its distinctive features and low cost (Gurunathan and Ravi, 2015; Liu and Zhang, 2011). Note that ZnO as a base metal oxide is a reactive metal promoter in the catalytic process of biodiesel. Baskar et al. (Baskar et al. 2018) conducted a conversion reaction on castor oil with high free fatty acid over a Ni-doped ZnO nanocatalyst under optimum conditions (biodiesel yield = 95.2%). As ZnO is a base promoter, a bifunctional acid-base catalyst may be synthesized by incorporating ZnO material on the surface of the support with acid sites. Furthermore, the presence of excellent catalytic activity of these catalysts with many strong acid-base sites is useful for promoting simultaneous esterification and transesterification.

Until now, the sulfonated biochar-based heterogeneous catalyst prepared from the insect shell for biodiesel production has been rarely reported. Here, a surfactant methodology was adopted to mediate the mesopores of sulfonated biochar support from the outset, which ensures spatial compartmentalization of chemically distinct active sites.

The molecular weight, polarity, and hydrophilicity of the introduction of polymer matters in the catalyst synthesis process influence the specific surface area and catalytic activity of the catalyst and result in composite catalyst with different morphologies and catalytic capacities (Du et al., 2019; Jeon et al., 2013). Based on the present studies, polyvinyl pyrrolidone (PVP) as a support mediator was introduced to improve the textural properties and catalytic capacity of the catalyst for the conversion reaction. This paper focused on the utilization of the insect shell for the development of a novel bifunctional acid-base catalyst (ZnO/PVP_{mediate}-BC-S) for the conversion of the insect lipid into biodiesel. The synergistic catalysis of both active acidic and basic sites will be an efficient and reusable approach for the production of biodiesel from renewable insect lipid to biodiesel with environmentally friendly. The physicochemical characterization of the synthesized composite catalyst was investigated. The influences of the composite catalyst preparation conditions and the catalytic reaction conditions on the biodiesel yield were also investigated. More importantly, the possible catalytic mechanism of the prepared catalyst was comprehensively described. Moreover, the reusability of the prepared catalyst during five reaction cycles was demonstrated and studied to evaluate its stability. Finally, the physicochemical properties of biodiesel were also studied.

2. Experimental section

2.1. Materials

The energy insect shells were collected from the Wuhan Institute of Technology (Fig. 1). The lipids extraction process is similar to that reported in our previous work (Feng et al., 2019). The fatty acid compositions of insect lipids were listed in Table 1. Besides, Zn(Ac)₂, NaOH, PVP, sulfuric acid, and methanol were analytical reagents and purchased from a local supplier in China.



Fig. 1 The insect shell used in the present study.

Table 1 The fatty acid compositions of insect lipid used in the present study.

Fatty acids	Proportion (%)
Capric acid (10:0)	1.30
Lauric acid (12:0)	18.89
Myristic acid (C14:0)	9.91
Palmitic acid (C16:0)	20.96
Stearic acid (C18:0)	6.50
Oleic acid (C18:1)	22.54
Linoleic acid (C18:2)	12.67

2.2. Catalyst preparation

2.2.1. Preparation of activated biochar

Briefly, the insect shell was first washed and dried in an oven at 80 °C overnight. Then, the shell was milled and sieved to obtain uniform-sized particles (80 mesh screen, average pore size ≈ 0.18 mm). Subsequently, appropriate masses of resultant particles and PVP (5–45% by weight, occupy the weight of insect particles) were introduced into the distilled H₂O. The resulting mixture was continuously stirred at 60 °C for 3 h. After treatment, the precipitate was separated and then calcined at different temperatures (300–700 °C) in a muffle furnace for 6 h. The carbonized product (denoted as PVP_{mediate}-BC) was later further treated with sulphuric acid

at 90 °C for 3 h. Immediately after that, the activated biochar was washed and dried at 100 °C overnight (denoted as PVP_{mediate}-BC-S).

2.2.2. Preparation of composite catalyst

Typically, the required amount of Zn(Ac)₂ (Zn(Ac)₂ concentration = 0.05 to 0.7 mol/L) and NaOH were dissolved in distilled water. Then the support (PVP_{mediate}-BC-S) was immersed in the mixture solution. Furthermore, the mixture was heated at 90 °C for 3 h. Finally, the resulting solid precipitate (ZnO/PVP_{mediate}-BC-S) was isolated from the solution and then dried at 80 °C for 12 h.

2.3. One-step synthesis of biodiesel from the insect lipid

The prepared solid catalyst was used to evaluate its catalytic performance in converting insect lipid into biodiesel. An appropriate amount of methanol (molar ratio of methanol/lipid = 3:1–15:1), catalyst (2–10% by weight), and 10 g of insect lipid are poured sequentially into a 250 mL flask. Then, the mixture was heated at 65 °C for 4 h. The reaction mixture was centrifuged to separate the solid catalyst after the reaction. The biodiesel yield was calculated based on a formula (1) (Zhao et al., 2018):

$$\text{Biodiesel yield}(\%) = \frac{\text{Weight of obtain biodiesel (g)}}{\text{Weight of insect lipid (g)}} \times 100\% \quad (1)$$

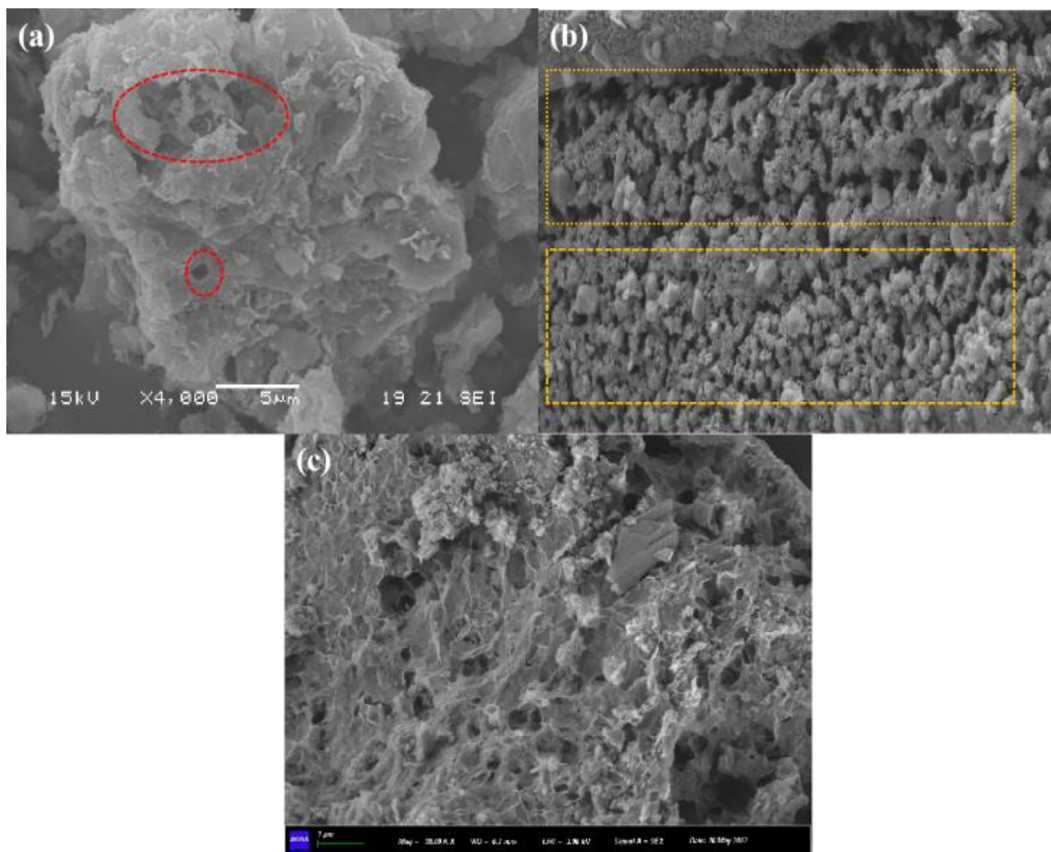


Fig. 2 SEM images of (a) raw BC-S support, (b) PVP_{mediate}-BC-S support, and (c) ZnO/PVP_{mediate}-BC-S catalyst.

2.4. Catalyst characterization

The morphologies of the prepared catalyst were investigated using scanning electron microscopy (SEM, JSM-7500, Japan). Transmission electron microscopy (TEM) images were recorded with a Tecnai G2 F20 S-TWIN microscope instrument. The structure and crystalline phase of the synthesized catalyst were determined using X-ray diffraction technique (XRD, Rigaku, Japan). The XRD patterns were recorded from 2θ of 10 to 60° . The XPS analyses were performed on an ultra-high-vacuum VG channel detector, using Al K α radiation (1486.7 eV). Surface functional groups of the catalyst sample were tested by Fourier transform infrared spectroscopy (FTIR, American Thermo Electron) with spectrum of 400–4000 cm^{-1} . The surface area of the prepared catalyst was evaluated by multi-point Brunauer-Emmett-Teller (BET) analysis with a Micromeritics ASAP 2020 nitrogen adsorption apparatus (USA). The pore volume and pore diameter were determined by the Barrett-Joyner-Halenda (BJH) method. ^1H NMR spectrum of insect lipid and biodiesel were recorded with CDCl_3 in FT-NMR spectrometer (Bruker Avance II). The basicity of the prepared catalyst was measured using Hammett indicators.

2.5. Statistical analysis

The catalytic reaction procedures were followed in duplicate. The experiment results were processed and analyzed by using a traditional editing software (origin pro 9.1, USA).

3. Results and discussion

3.1. Synthesis and physical characterization of the composite catalyst

3.1.1. Surface morphology characteristic

Fig. 2 depicts the mesoscopic morphological characteristics of raw biochar support, PVP_{mediate}-BC-S support, and ZnO/PVP_{mediate}-BC-S catalysts. The presence of a few pores on the surface of raw biochar support is shown in Fig. 2a. Meanwhile, it is interesting to find that there are some discrete pores

of various sizes on the surface of PVP_{mediate}-BC-S support when PVP was used as a support mediator (Fig. 2b). The results of this study indicated that high molecular polymer mediation was effective in improving the porous properties of biochar support and was also a prominent technique for realizing hierarchical pore structure in support. However, it is clear that the pores on the support surface were blocked due to the dispersion of the ZnO materials from Fig. 2c. It can thus be concluded that ZnO materials have been successfully dispersed in the biochar-based support.

3.1.2. Surface area analysis

The textural properties of the prepared catalyst were further investigated via N_2 adsorption–desorption isotherms (Fig. 3).

The prepared catalyst shows H3-hysteresis and a typical IV isotherm, indicating the formation of a predominantly mesoporous structure (Fig. 3). A significant increase was observed at a relatively high P/P_0 (0.8–1.0), indicating the presence of capillary structures (Fig. 3a). Furthermore, based on these observations, it is speculated that the synthesized catalyst had uniform pores. The primary requirement for an ideal conversion reaction in the presence of solid catalysts is the pore structure. The pore diameter fractions of raw biochar (BC-S) are 5–10 nm, according to BJH desorption isotherms (Fig. 3b). The average pore diameter and pore volume of raw BC-S were 8.79 nm and 0.0821 cm^3/g , respectively (Table 2). Clearly, the pore diameter fractions and surface area are increased after PVP mediation. The pore size distribution revealed that the PVP_{mediate}-BC-S support had more mesopores. The SEM micrographs also revealed these changes. Furthermore, after loading ZnO material on the support, there is a slight decrease in pore volume and pore diameter. This could be attributed to the fact that the surface of catalyst support was covered upon ZnO active components and the pores of the catalyst were blocked, which in turn caused the decrement in pore properties.

3.1.3. Structure and crystallography

The typical XRD pattern obtained from ZnO/PVP_{mediate}-BC-S is displayed in Fig. 4. The peaks at $2\theta = 31.5^\circ, 34.2^\circ, 36.3^\circ, 47.35^\circ,$ and 56.3° , indicate (100), (002), (101), (102), and (110) crystalline phases in the ZnO structure (JCPDS

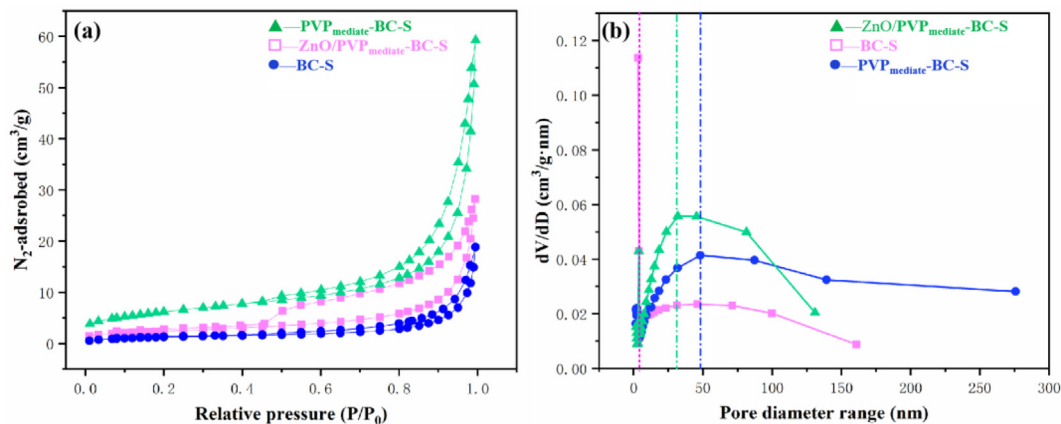


Fig. 3 N_2 adsorption–desorption isotherms and pore size distribution of raw biochar (BC-S), PVP_{mediate}-BC-S support, and ZnO/PVP_{mediate}-BC-S catalyst.

Table 2 Pore textural properties of the prepared products.

Sample	Surface area (m ² /g)	Pore diameter (nm)	Pore volume (cm ³ /g)
BC-S	11.12	8.79	0.0821
PVP _{mediate} -BC-S	25.46	19.12	0.0732
ZnO/PVP _{mediate} -BC-S	18.38	13.33	0.0627

36-1451), respectively (Lokhande et al., 2009). The appearance of peaks associated with the synthesized biochar at $2\theta = 10-30^\circ$ and $2\theta = 40-50^\circ$ can be readily indexed to (002) and (101) crystalline phases, respectively (Wang et al., 2018). According to Aziz et al. (Aziz et al., 2015), the broad peaks ($2\theta = 10^\circ-30^\circ$) can be well assigned to those of amorphous carbon. Zhao et al. (Zhao et al., 2009) mentioned that the C—O—C cleavage bonds of the biochar precursor were disrupted by the synergistic interaction between the carbonization process at high temperature and the sulfonation process. The sulfonated carbon became more rigid and amorphous due to the high degree of carbon disorder during this process. Hence, this structural modification of the sulfonated carbon catalyst is an important step that is responsible for the efficiency of the catalytic reaction in this study.

3.1.4. TEM

The structural information of the synthesized catalyst has been further examined by TEM observation, and some representative images are presented in Fig. 5. According to Fig. 5a, the polymer functionalization approach used in this study can introduce a significant number of mesopores with worm-holes into BC support. In addition, the lattice fringes on the surface region correspond to the (110) plane of ZnO. This finding suggests that ZnO material is well loaded on the

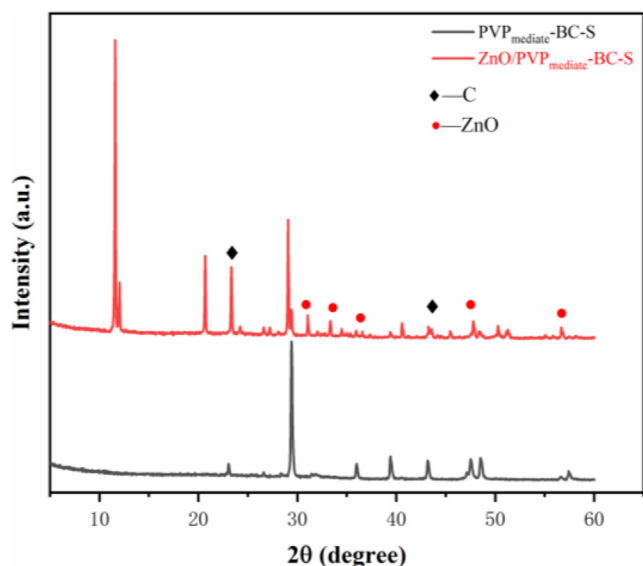


Fig. 4 XRD patterns of the PVP_{mediate}-BC-S support and ZnO/PVP_{mediate}-BC-S catalyst.

surface of the biochar-based support (Fig. 5b) (Malhotra and Ali, 2019; Kazmi et al., 2020).

3.1.5. FT-IR

The FT-IR analysis of the functional group bond on the support surface was presented in Fig. 6. The broad absorption band at around 1426.89 cm^{-1} can generally be assigned to the aromatic ring C=C stretching mode of carbonate species (Hsiao et al., 2011). Moreover, the bands at 1120 cm^{-1} are related to the symmetric stretch of the $-\text{SO}_3\text{H}$ bond, present in the structure of the sulfonic groups (Zong et al., 2007). It should be pointed out that the sulfoxide group still exists on the synthesized carbon support, although the support was washed three times during the end of the pretreatment process. This finding suggests the successful grafting of $-\text{SO}_3\text{H}$ groups onto the carbon support after the sulfonation process for the application in catalytic reaction (Sangar et al., 2019). In addition, two characteristic peaks at 601.99 and 670.74 cm^{-1} were attributed to the stretching vibrations of Zn—O (Zhang et al., 2009).

3.1.6. XPS

The surface chemical composition of the prepared sample was further investigated by using XPS analysis (Fig. 7). The peak at 169 eV is ascribed to the sulfur of $-\text{SO}_3\text{H}$ groups (Song et al., 2020). These indicate that the $-\text{SH}$, $-\text{SO}_3\text{H}$ groups are present in the prepared composite catalyst. The two peaks in the spectrum of C 1s (Fig. 7) at 285.01 eV and 288.2 eV represent the binding energies of carbon of carbonates present in the catalyst (Pan et al., 2020). The predominant chemical states in ZnO materials are oxygen (O 1s) and Zinc (Zn 2p). There is one peak with a binding energy of 531.11 eV (O 1s) associated with the elemental oxygen of oxides present in the catalyst (Medeiros et al., 2020). Furthermore, the peak at 1022.1 eV (Zn 2p) is associated with Zn in the zinc oxide (Feng et al., 2016). These binding energies fit well with the chemical bonding structure of the composite catalyst.

3.2. Catalyst performance

The synthesized catalyst was applied to the catalytic reaction of the insect lipid. Here, a series of experiments were performed to test the effects of different conditions on catalytic performance.

3.2.1. Effect of carbonization temperature

The carbonization temperature was investigated to optimize the synthesis of catalysts for higher biodiesel yield. As seen in Fig. 8a, the biodiesel yield increases with the increase in carbonization temperature from 300 to $600\text{ }^\circ\text{C}$ (from 57.14% to 94.36%). The carbonization at higher temperature led to the desorption of CO_2 from the insect shell support, producing more pores that catalyzed the transesterification of insect lipids. Additionally, the surface area of the catalyst could be affected by carbonization temperature, which consequently affects the efficiency of the catalyst. Moreover, it is also found that the catalytic capacity of the catalyst (86.68%) decreased with the further increase in the carbonization temperature. This can contribute to both the high sintering rate of the catalyst and the high energy consumption (Obadiah et al., 2012).

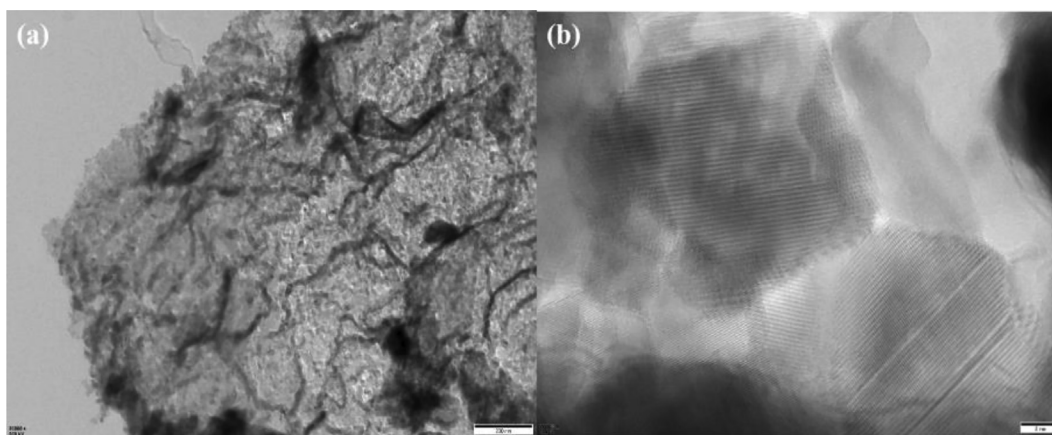


Fig. 5 TEM images for the synthesized catalyst.

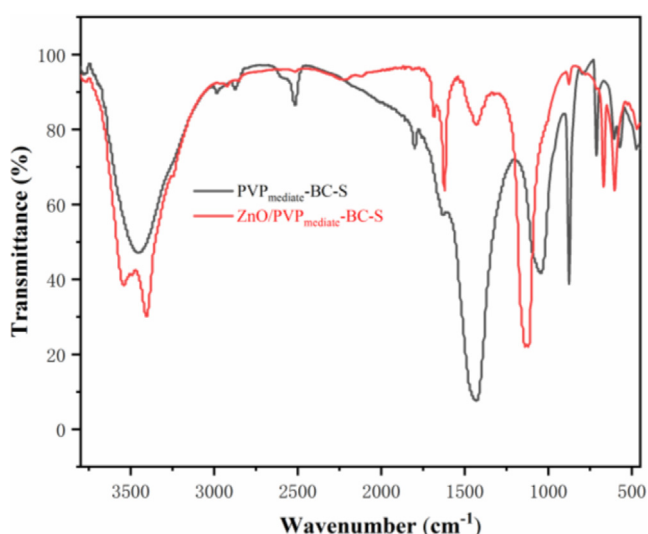


Fig. 6 FT-IR analysis of the PVP_{mediate}-BC-S support and ZnO/PVP_{mediate}-BC-S catalyst.

3.2.2. Effect of ZnO loading

A series of experiments were carried out by altering Zn(Ac)₂ concentrations to investigate the influence of ZnO loading on the catalytic process (Fig. 8b). Remarkably, with this increasing Zn(Ac)₂ concentration (0.05 to 0.7 mol/L), the biodiesel yield gradually increased from 52.66% to 94.36%. However, there was no noteworthy increase in conversion yield with Zn(Ac)₂ concentration beyond 0.3 mol/L. The reason for this result can be deduced from the crystallization or agglomeration of ZnO materials which resulted in poor dispersion of active components on the surface of the support (Tantirungrotechai et al., 2013). Meanwhile, according to the Hammett indicator method results, the catalyst with 0.3 mol/L Zn(Ac)₂ concentration had the strongest basicity. With the catalytic activity of samples, it could be concluded that high basicity could contribute to a higher biodiesel yield.

3.2.3. Effect of PVP amounts

It is evident from this work as well as from literature that the polymer amounts can have a pronounced effect on pore

textural properties of the prepared catalysts, and therefore play a key role in the catalytic performance. We can see that the pore size of the catalyst is primarily distributed at 10–19 nm for the synthesized catalyst with PVP as a structural medication agent (Table 3).

Since the pore size of the synthesized catalyst is larger than that of the triglyceride molecule (58 Å), the triglyceride molecule would react with the active component on the surface or in the channel of support (Li et al., 2019). The biochar support by PVP-mediated had a significant influence on the catalyst, whereas the catalyst without PVP had a smaller specific surface area and pore volume (Fig. 9). Based on these observations, this is presumed to be due to the introduction of appropriate PVP intensifying the dispersion of active components on the surface of the catalyst (Margellou et al., 2018). The other possible reason is that the organic polymer with free radical structures and organic groups such as Lewis acids could withdraw or donate electrons (Figueiredo et al., 2007). It has been reported in the literature that the carbonyl/quinone groups on the surface of carbon are the strong active sites for oxidative dehydrogenation reactions (Pereira et al., 1999). Following a further increase in PVP amount (beyond 35 wt%), no appreciable improvement in biodiesel yield was seen. One possible explanation for this phenomenon is that the excessive organic calcination residues on the surfaces of support may lead to a significant decrease in the pore volume and pore size of support (Qu et al., 2021). This phenomenon in this study is similar to that reported in other previous literature (Guisnet and Magnoux, 2001; Moreno-Castilla et al., 2001). Nevertheless, the mechanism by which the organic polymer assisting improves catalytic performance remains unclear. Thus, further investigations are required to uncover this mechanism, and this is the next step in our future studies.

3.2.4. Effect of catalyst loading

The catalytic reactions were carried out by varying the loading of the synthesized catalyst (Fig. 10a). It is interesting to notice that the conversion yield can reach 65.37% even at lower catalyst loading. The biodiesel yield increased progressively with increasing in the catalyst loading. Thus, the biodiesel yield of 94.36% could be achieved when the catalyst loading was 6 wt%. The increase in biodiesel yield with increasing loading of the catalyst was due to the increase of active sites of the

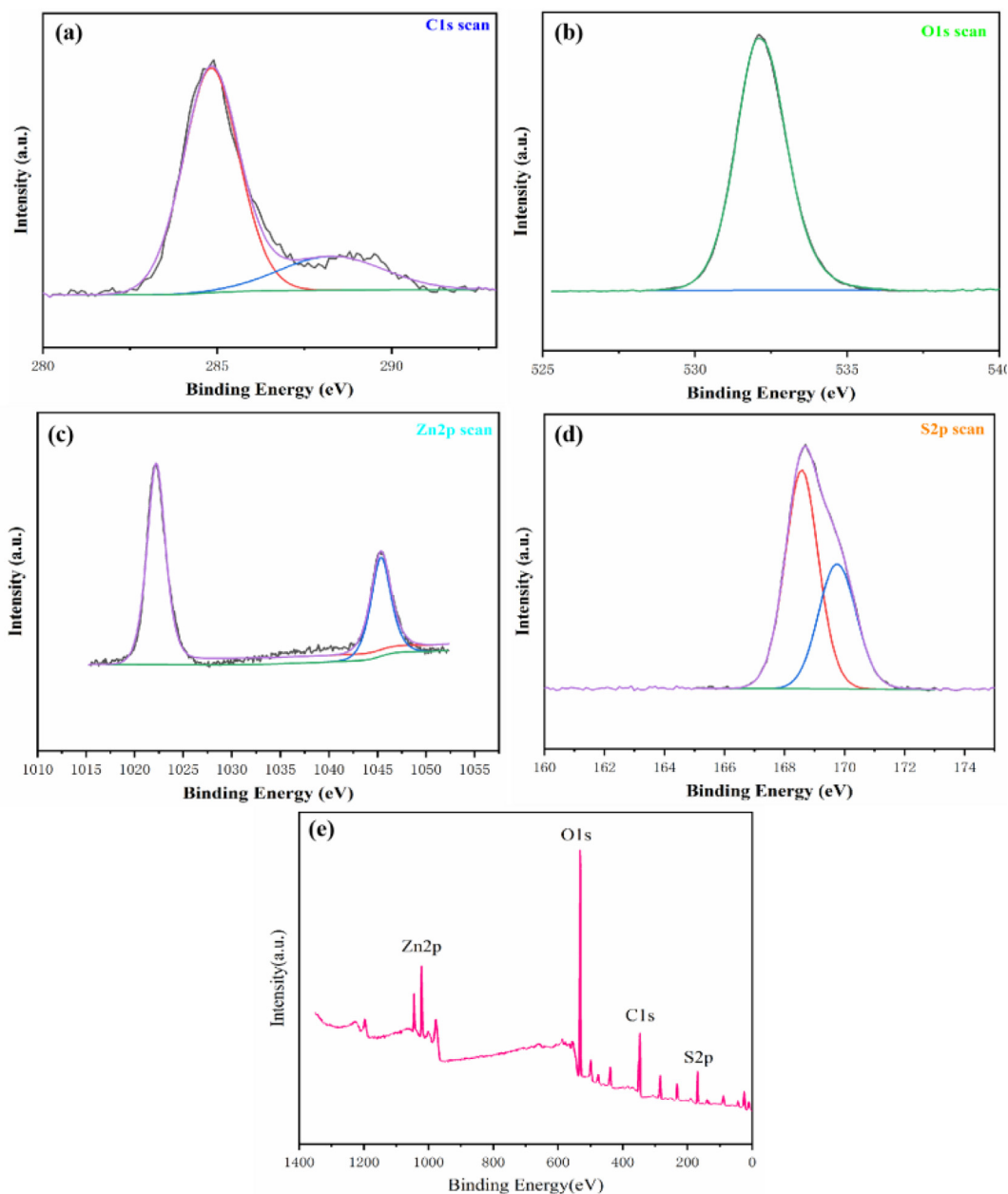


Fig. 7 XPS analysis of the synthesized catalyst.

catalyst participated in the conversion reaction. Moreover, the biodiesel yield decreased with increased catalyst loading by more than 6 wt%. There are two possible reasons caused the decrease in biodiesel yield at a higher catalyst loading: (1) The higher catalyst loading may lead to the increase of the viscosity in the mixture reaction system, which has influenced the mass transfer between the reactants and the catalyst (Negm et al., 2017; Hwa et al., 2015). (2) ZnO catalyst is an amphoteric composite, the saponification side reaction might have induced resulting in decreasing biodiesel yield (Santana et al., 2012).

3.2.5. Effect of methanol amount

The catalytic reactions of the insect lipid were conducted at methanol to lipid molar ratio of 3:1–15:1 (Fig. 10b). The

lowest conversion of lipid into biodiesel (34.22%) was obtained when the molar ratio of methanol to lipid was 3:1. It is evident from Fig. 10b that the biodiesel yield increases linearly with methanol amount. The biodiesel yield of lipid was 94.36% at a methanol/lipid molar ratio of 9:1. However, the biodiesel yield decreases slightly when the molar ratio of methanol/lipid exceeded 9:1. But at a higher molar concentration of methanol, there were two possibilities for reducing biodiesel yield: (1) Due to the reversible nature of the *trans*-esterification reaction, the equilibrium of reaction has shifted toward the backward reaction (Bhatia et al., 2020; Mutreja et al., 2014). (2) Additionally, further excess deluges the active sites of the catalyst that may hinder the protonation of fatty acid at the active sites, resulting in a decrease in biodiesel yield (Khan et al., 2020; Roy et al., 2020).

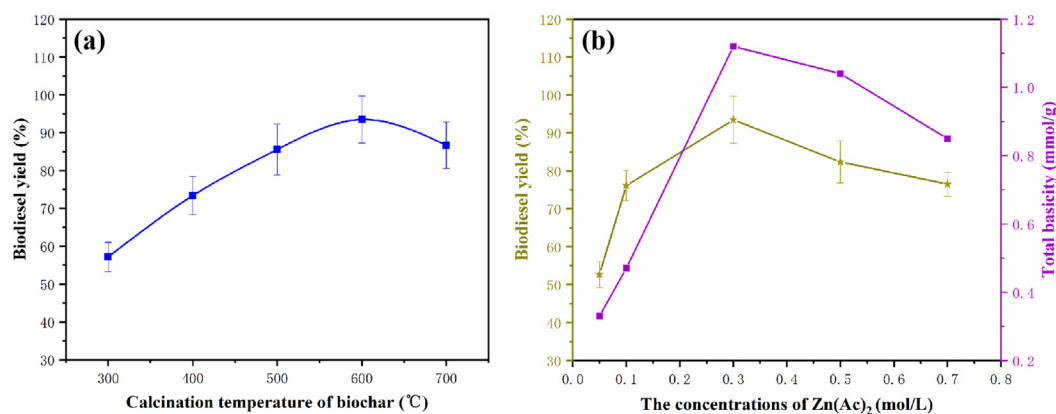


Fig. 8 The effect of the different preparation conditions on the biodiesel yield. a-carbonization temperature; b-ZnO loading.

Table 3 Pore textural properties of the prepared products with different PVP amounts.

Sample	Surface area (m ² /g)	Pore diameter (nm)	Pore volume (cm ³ /g)
0	11.12	8.79	0.0821
5%	12.29	10.13	0.0798
15%	16.14	14.78	0.0786
25%	20.66	16.23	0.0771
35%	25.46	19.12	0.0732
45%	17.26	17.68	0.0714

considering that the high temperature condition is helpful to increase the probability of effective collisions between the catalyst and the reactant molecules, resulting in a faster rate of mass transfer, hence resulting in increased conversion yield of biodiesel (Sahani et al., 2019). At the higher temperature (65 °C), a conversion yield of 94.36% was obtained. However, a slight decrease in the biodiesel yield was observed when the reaction temperature exceeded 65 °C under the same reaction conditions. This phenomenon occurred because of the vaporization of the excess methanol at the optimal temperature (Saravanan et al., 2015).

3.2.7. Effect of the alcohol types

The effect of alcohol types in the conversion reaction is shown in Fig. 10d. Using the prepared catalyst, the biodiesel yield decreases with increasing alcohol molecular weight. The order of the conversion capacity is methanol, ethanol, propanol, isopropanol, and *tert*-butanol. The reason was ascribed to the fact that the larger alcohol chains have inferior nucleophilicity. By comparing the decomposition capacity of other alcohol, methanol with more nucleophilicity of methoxide ion decomposes more quickly (Basumatary et al., 2021). In addition, larger chains have a greater steric hindrance, which prevents fatty acids from interacting with the catalyst (Araujo et al., 2019).

3.3. Reusability and stability of catalyst

As regards the homogeneous catalyst, the most intriguing feature of this heterogeneous catalyst is that it still had high catalytic activity and stability after successive reaction cycles. Therefore, further recycling experiments were performed using the synthesized catalyst under the defined conditions to evaluate the reusability of the catalyst (Fig. 11). Upon completion of each reaction, the solid was collected and directly reused in subsequent cycles. The second catalytic reaction was carried out under the previous same conditions and a conversion yield of 88.66% was obtained. This procedure was repeated five times. It is noticeable that there appears to be no significant decrease in biodiesel yield for each repeated experiment. There are three possible reasons caused the decrease in the activity of the catalyst. (1) The loading of catalyst used in the next cycle was lower than the initial cycle, which might partly be respon-

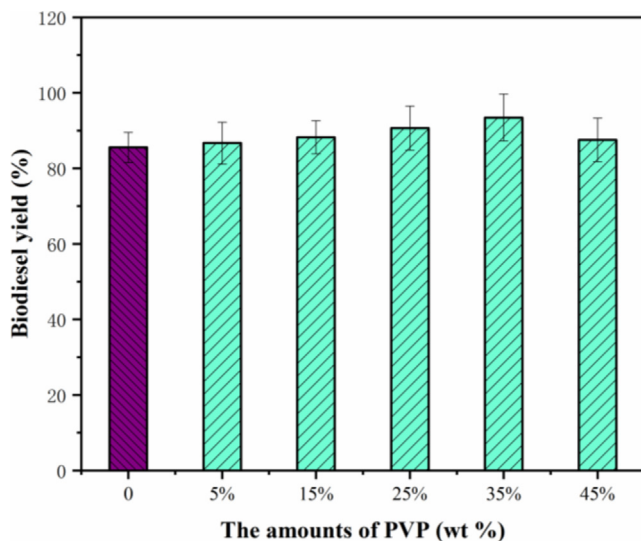


Fig. 9 The effect of PVP amounts on the biodiesel yield.

3.2.6. Effect of catalytic reaction temperature

To evaluate the effect of the catalytic reaction temperature, the catalytic reaction was conducted at different ranges of temperature (Fig. 10c). It is thus apparent that the biodiesel yield increased with increasing the reaction temperature. The reason for this result can be deduced from the mass transfer principle

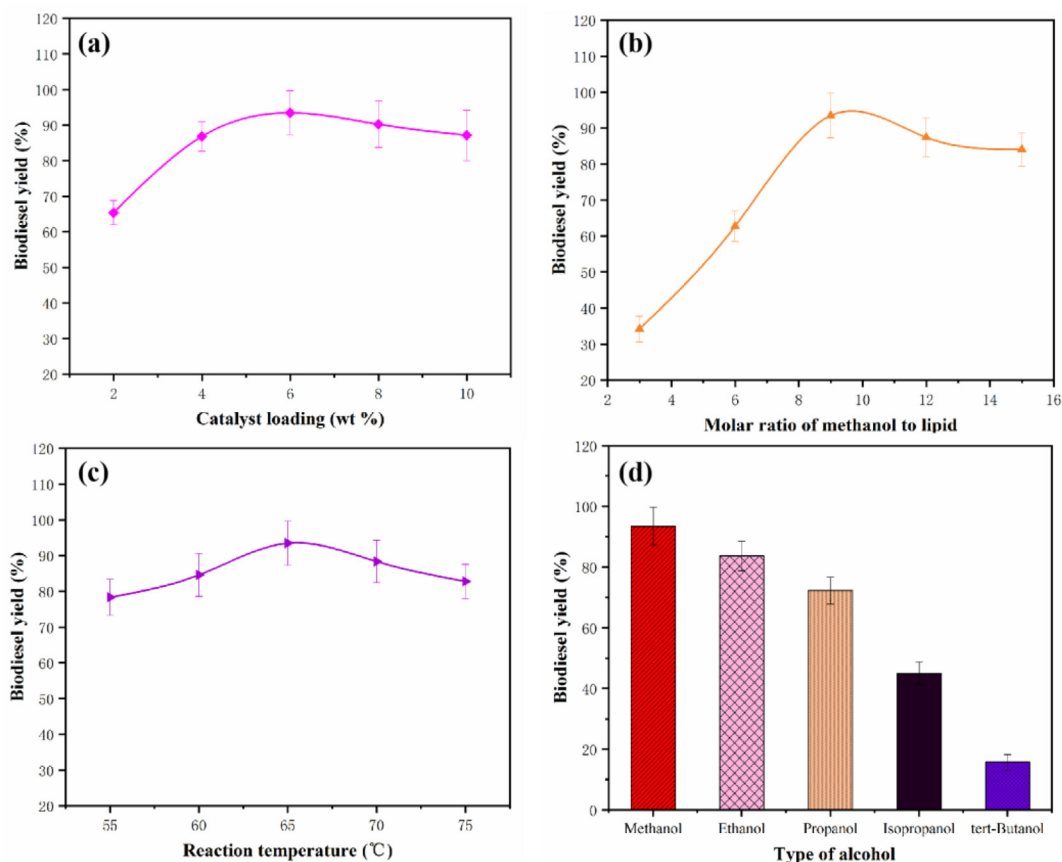


Fig. 10 The effect of reaction conditions on the biodiesel yield. a-catalyst loading; b-methanol amount; c-catalytic reaction temperature; d-alcohol types.

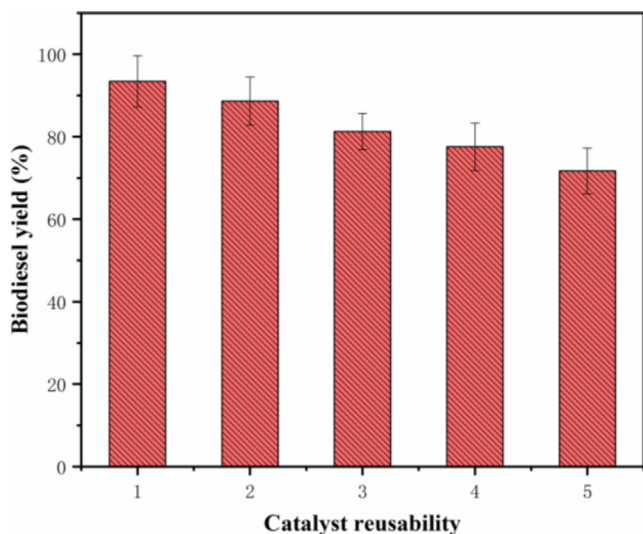


Fig. 11 Reusability of the synthesized catalyst.

sible for reducing biodiesel yield during the recycling experiments. (2) The produced by-product glycerol covered the surface of the catalyst and blocked the active sites of the catalyst (Gohain et al., 2020). (3) The leaching of active components of the catalyst would lead to the decrease of catalytic activity during the recycling experiments (Khan et al., 2020).

To further explore the feasibility of the synthesized catalyst, the characterizations of SEM and TEM were carried out for the fresh and reused catalyst (five cycles). The SEM (Fig. 12a) micrograph shows that the synthesized catalyst retains its bulk-like nanostructure. Compared with Fig. 2(c) and Fig. 5(a), it is likely that the surface and porous structure of the synthesized catalyst changed slightly. The change in the surface and porous structure of the synthesized catalyst was due to the catalyst being poisoned by the irreversible adsorption of the free fatty acids on the active sites, which destroys the pore structure and increases the mass transfer resistance (Kwong and Yung, 2016; Li et al., 2022).

Meanwhile, combining Fig. 13(a) with Fig. 13(b), there was no obvious apparent difference in the structure and the physicochemical properties of the reused catalyst after five cycles. However, there was a significant decrease in the peak intensity of ZnO after the reused reaction, implying the loss of active components during each reaction. Besides, the newly detected functional groups (2920 and 2850 cm^{-1} , C—H stretching vibration of glycerol molecule) on the reused catalysts, may block the active sites and result in reduced activity on the reused catalyst (Yusuff et al., 2021). Consequently, the biodiesel yield decreased as the reaction cycle increased. Further work is ongoing to optimize the composite catalyst to limit the decrease in the yield of biodiesel in the subsequent cycles of use.

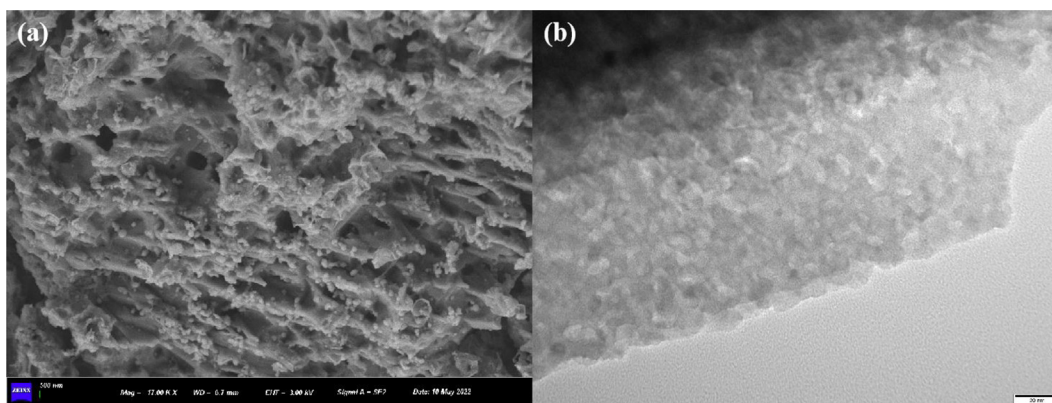


Fig. 12 SEM and TEM of the reused catalyst.

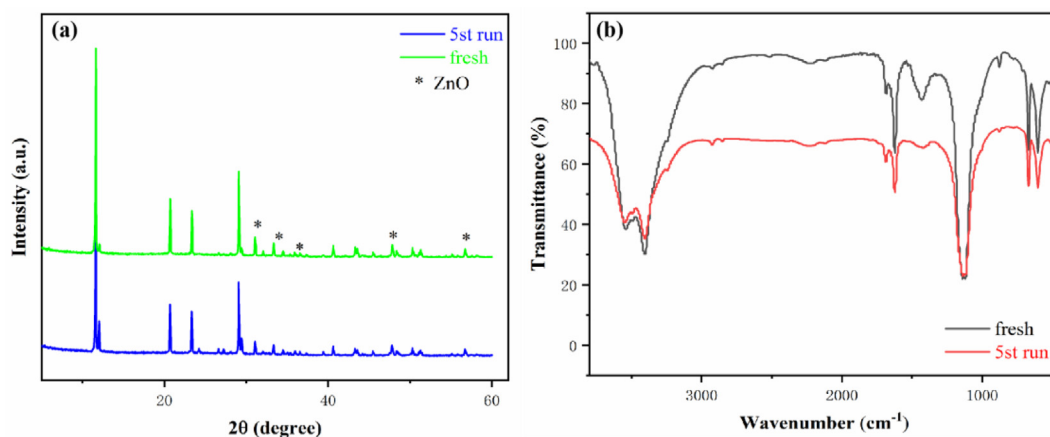


Fig. 13 XRD pattern and FT-IR spectra of the fresh and reused catalyst.

In comparing the catalytic activity of those previously reported catalysts, it is clear that the synthesized catalyst has better stability and reusability for biodiesel production in the current work (Table 4). For instance, biodiesel yield reduced from 94.36% to 47.52% after the fifth cycle when corncob biomass waste-based acid catalyst was utilized as an efficient catalyst in the transesterification of palm fatty acid (Tang et al., 2020). Macawile et al. reported that biodiesel yield decreased from 93.10% to 58.09% after the third cycle of reuse of the novel modified solid acid catalyst (Macawile et al., 2020).

3.4. Catalytic mechanism of the prepared catalyst

The ZnO materials were loaded on the sulfonated biochar-based support in this study. As both acid and base groups

are present on the surface of the biochar support, both acid-base mechanisms are likely to occur. Fig. 14 depicts the proposed mechanism simplified for the catalytic reaction.

Acid catalysis: The first step involves protonation of the carbonyl group of insect lipids by the protons generated from the acidic sites. The sulfonate groups ($-\text{SO}_3\text{H}$) on the framework of the prepared catalyst have labile hydrogen protons that can be easily migrated to attack the most nucleophilic centers of lipids ($\text{C}=\text{O}$) to form the protonated form of lipids (Macawile et al., 2020). Then, the electron-rich hydroxyl groups of methanol would nucleophilic attack the cationic centers on protonated lipid (Betiha et al., 2020). The unstable protonated lipid-methanol ether complex formed undergoes two successive stabilization steps. The first includes the loss of water molecules to produce the protonated lipid-methanol ester intermediate. The second involves the conversion of the

Table 4 Comparison of catalytic performance of different supports used for biodiesel production.

Support	Feedstock	BY	Cycles	Reference
Corn cob biomass waste	Palm fatty acid	47.52%	5	Tang et al. (2020)
Functionalized carbon nanotubes	High free fatty acid	58.09%	3	Macawile et al. (2020)
Li-doped activated carbon	Mixture of non-edible oils	67.66%	6	Ayoob and Fadhil (2019)
Banana peel ash	Soybean oil	52.16%	4	Pathak et al. (2018)
Jatropha curcas biomass	Jatropha curcas oil	81.03%	4	Mardhiah et al. (2017)

BY-Biodiesel yield.

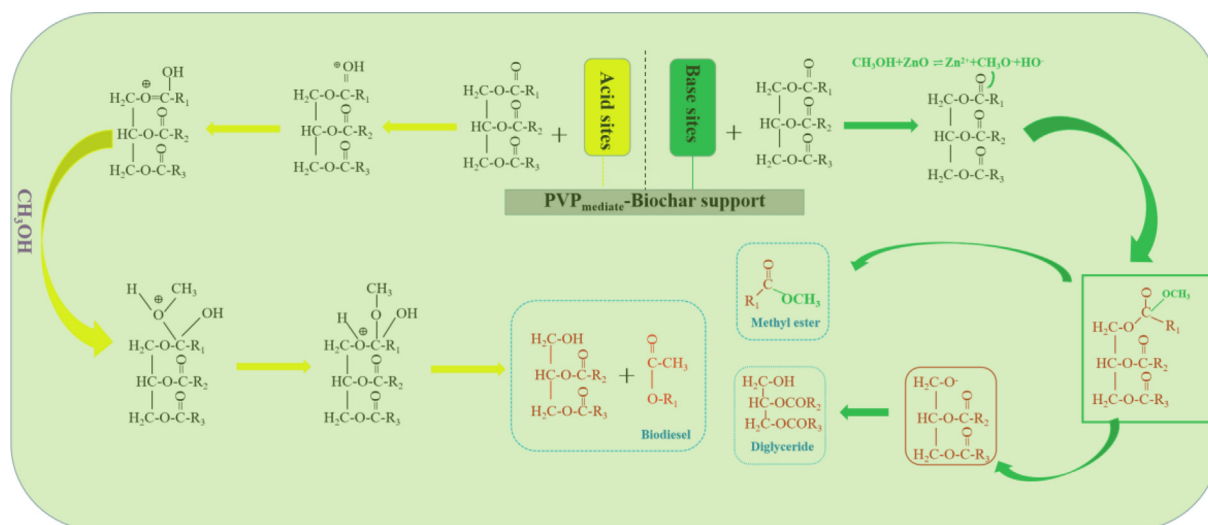


Fig. 14 Catalytic mechanism of the synthesized catalyst.

protonated lipid-methanol ester intermediate into the corresponding lipid-methanol ester by losing protons, which are combined with the ionized acidic catalysts to retain their chemical structures (Khan et al., 2021).

Base catalysis: The two types of esterification and transesterification simultaneously took place on the surface of the biochar-based catalyst. ZnO as a Brønsted base was loaded on the support during the catalysis process. A part of methanol and triglyceride reactants may be adsorbed at different Zn active sites on the ZnO catalyst surface. Thus, it was reasonable that the interaction of the ZnO catalyst and triglyceride would form the bond of Zn and $-O-CH_2$. The presence of ZnO in the chemical structure of the catalyst has a high influence on its alkalinity (Kouzu et al., 2009; Putra et al., 2018). The fatty acid methyl ester is then produced and formed diglyceride. The diglyceride further reacted with methanol to produce the object product (fatty acid methyl ester) and intermediate (monoglyceride). In the meantime, the monoglyceride is further involved in the reaction to form fatty acid methyl ester and by-product (glycerol). Finally, the by-product glycerol may be desorbed from the active sites of the biochar-based catalyst. In this way, the catalyst can be reused in subsequent reactions.

3.5. Analyses of biodiesel produced

3.5.1. FT-IR spectra analysis

Fig. 15a shows the FTIR spectra of insect lipids and biodiesel. The absorption band at 3400 cm^{-1} for insect lipids, which indicates the occurrence of $(-OH)$ stretching vibration of carboxylic acid, alcohol, or phenol (Ayoob and Fadhil, 2019). Interestingly, the observed absorption band disappears in the FTIR spectra of biodiesel. Its absence in biodiesel indicates that esterification has been highly effective. As shown in Fig. 14a, the biodiesel spectra have two sharp and broad peaks at 2920 cm^{-1} and 2851 cm^{-1} , respectively. The bands at $2920\text{--}2851\text{ cm}^{-1}$ are due to symmetric and C-H asymmetric stretching vibrations (Falowo et al., 2020; Falowo and Betiku, 2022). The C=O stretch vibration at 1745 cm^{-1} of insect lipid shifts to 1742 cm^{-1} in biodiesel, which represents the conversion

reaction (Ayoob and Fadhil, 2020). The peak at 1461 cm^{-1} corresponds to the bending of CH_2 (Li et al., 2015). A peak at 720 cm^{-1} was observed and assigned to the vibration of the CH_2 bond from the long fatty acid chain (Li et al., 2019). The existence of major absorption bands proved that biodiesel was produced in this work. The results obtained in this study were in good agreement with those reported in the previous study (Tsanaktsidis et al., 2013).

3.5.2. 1H NMR analysis

The synthesis of biodiesel from insect lipids was characterized by the 1H NMR spectra (Fig. 15b). The major differences in signals indicated the conversion of insect lipids to biodiesel. In Fig. 13b, the peaks present at 4.28 ppm and 5.33 ppm correspond to the glyceridic protons and olefinic protons ($-CH=CH-$) in insect lipids, respectively (Fadhil et al., 2019). A new singlet observed on the spectra around 3.57 ppm indicates the appearance of methoxy protons ($-CO-OCH_3$) (Li et al., 2015). Instead, the glyceridic peaks near 4.28 ppm completely disappeared. The results observed here illustrated that the insect lipid was successfully converted to biodiesel. The signals at 2.30 ppm in the 1H NMR spectrum of insect lipid and 2.22 ppm in the 1H NMR spectrum of biodiesel are due to $\alpha-CH_2$ protons to the ester ($-CH_2-CO_2R$) groups present in the insect lipid and biodiesel, respectively (Macina et al., 2019). The 1H NMR signals of the methylene $-(CH_2)_n-$ protons of the fatty acid chain in the insect lipid and biodiesel are observed at 1.25 ppm and 1.18 ppm, respectively (Nath et al., 2019). The terminal methyl protons ($-CH_3$) of the triglycerides and biodiesel are indicated by the 1H NMR signals at 0.87 ppm and 0.81 ppm, respectively.

3.6. Physicochemical properties of obtained biodiesel

The physicochemical properties of the biodiesel sample obtained from the conversion of the insect lipid over the prepared catalyst were determined and listed in Table 5. It can be noted that most of the fuel properties of biodiesel produced in this paper meet the specifications of the ASTM standard. Biodiesel with low viscosity is preferable for better com-

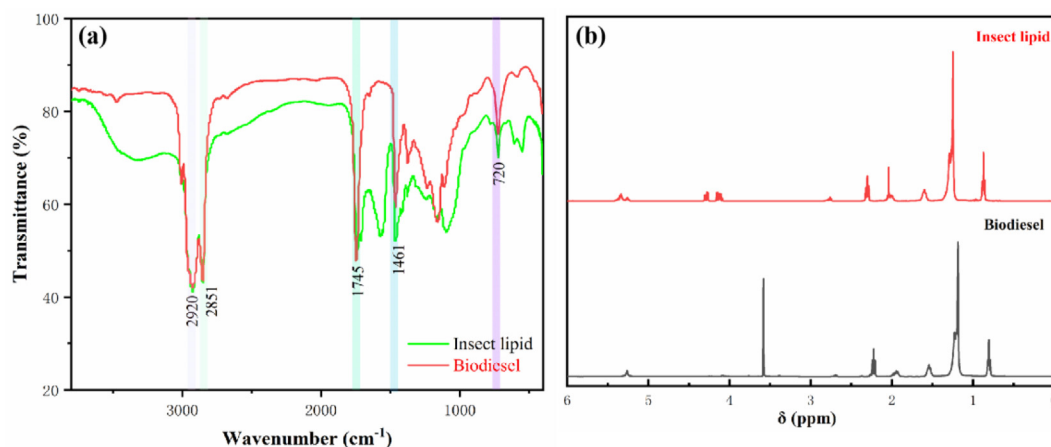


Fig. 15 FT-IR spectra and ^1H NMR spectra of the insect lipid and biodiesel.

Table 5 Physicochemical properties of obtained biodiesel.

Property	ASTM ^a	Insect lipid	Waste cooking oil ^b	Waste frying oil ^c	Fried oil ^d
Density (kg/m ³)	860–900	893	875	880	/
Viscosity (mm ² /s)	1.9–6.0	14.53	5.63	4.02	4.98
Pour point (°C)	–15 to 16	–5.0	–9	3	/
Acid value (mg KOH/g)	≤0.5	0.78	/	1.76	0.27
Moisture content (mg/kg)	< 500	413	400	/	766

^a Ref. Soltani et al. (2021).

^b Ref. Mansir et al. (2017).

^c Ref. Singh et al. (2016).

^d Ref. Viola et al. (2012).

bustibility in the engine. The viscosity reported in this study was well below the maximum limits of the ASTM standard. It is interesting to note that measurements of other fuel properties (acid value, density, and moisture content) from insect lipids derived from biodiesel were similar to the previously reported results.

4. Conclusions

In summary, a novel biochar-based heterogeneous catalyst (ZnO/PVP_{mediate}-BC-S) with acid-base bifunctional catalytic capacity was successfully synthesized by using PVP as a support mediator for the conversion of the insect lipid into biodiesel. The results of these experiments suggested that the biodiesel yield was 94.36% at the defined condition. As a mediator, PVP has enhanced the interaction between active components and support in the catalyst synthesis process. The appropriate PVP amount will be beneficial for the catalyst to have greater structure and crystallography of support, to maintain better catalytic activity. Meanwhile, the biodiesel yield did not decrease significantly after five cycles of reuse, indicating excellent stability and reusability of the prepared catalyst. Most of the fuel properties of the prepared biodiesel in this paper meet the ASTM standard specifications. This work demonstrates that biodiesel production with high yield catalyzed by inexpensive and facily fabricated biochar support from the waste insect shell has tremendous potential for large-scale production and practical applications.

Declaration of Competing Interest

The authors declare that they have no known competing financial interests or personal relationships that could have appeared to influence the work reported in this paper.

Acknowledgements

This work was financially supported by the Open Project of Beijing Key Laboratory for Enze Biomass and Fine Chemicals, Chongqing Key Laboratory of Soft-Matter Material Chemistry and Function Manufacturing (No. 20210005), Hubei Key Laboratory of Novel Reactor and Green Chemical Technology (No. NRG202209).

References

- Araujo, R.O., Chaar, J.S., Queiroz, L.S., Filho, G.N.R., Costa, C.E. F., Silva, G.C.T., Landers, R., Costa, M.J.F., Gonçalves, A.A.S., Souza, L.K.C., 2019. Low temperature sulfonation of acai stone biomass derived carbons as acid catalysts for esterification reactions. *Energ. Convers. Manage.* 196, 821–830. <https://doi.org/10.1016/j.enconman.2019.06.059>.
- Ayoob, A.K., Fadhil, A.B., 2019. Biodiesel production through transesterification of a mixture of non-edible oils over lithium

- supported on activated carbon derived from scrap tires. *Energ. Convers. Manage.* 201, 112149. <https://doi.org/10.1016/j.enconman.2019.112149>.
- Ayoob, A.K., Fadhil, A.B., 2020. Valorization of waste tires in the synthesis of an effective carbon based catalyst for biodiesel production from a mixture of non-edible oils. *Fuel* 264, 116754. <https://doi.org/10.1016/j.fuel.2019.116754>.
- Aziz, M.A.A., Jalil, A.A., Triwahyono, S., Ahmad, A., 2015. CO₂ methanation over heterogeneous catalysts: recent progress and future prospects. *Green Chem.* 17, 2647–2663. <https://doi.org/10.1039/C5GC00119F>.
- Baskar, G., Selvakumari, I.A.E., Aiswarya, R., 2018. Biodiesel production from castor oil using heterogeneous Ni doped ZnO nanocatalyst. *Bioresource Technol.* 250, 793–798. <https://doi.org/10.1016/j.biortech.2017.12.010>.
- Basumatary, B., Basumatary, S., Das, B., Nath, B., Kalita, P., 2021. Waste Musa paradisiaca plant: An efficient heterogeneous base catalyst for fast production of biodiesel. *J. Clean. Prod.* 305, 127089. <https://doi.org/10.1016/j.jclepro.2021.127089>.
- Betiha, M.A., Negm, N.A., El-Sayed, E.M., Mostafa, M.S., Menoufy, M.F., 2020. Capability of synthesized sulfonated aromatic cross-linked polymer covalently bonded montmorillonite framework in productivity process of biodiesel. *J. Clean. Prod.* 261, 120995. <https://doi.org/10.1016/j.jclepro.2020.120995>.
- Bhatia, S.K., Gurav, R., Choi, T.R., Kim, H.J., Yang, S.Y., Song, H. S., Park, J.Y., Park, Y.L., Han, Y.H., Choi, Y.K., Kim, S.H., Yoon, J.J., Yang, Y.H., 2020. Conversion of waste cooking oil into biodiesel using heterogeneous catalyst derived from cork biochar. *Energ. Convers. Manage.* 302, 122872. <https://doi.org/10.1016/j.biortech.2020.122872>.
- Cipolletta, M., D'Ambrosio, M., Moreno, V.C., Cozzani, V., 2022. Enhancing the sustainability of biodiesel fuels by inherently safer production processes. *J. Clean. Prod.* 344, 131075. <https://doi.org/10.1016/j.jclepro.2022.131075>.
- Costa, M.W., Oliveira, A.A.M., 2022. Social life cycle assessment of feedstocks for biodiesel production in Brazil. *Renew. Sust. Energ. Rev.* 159, 112166. <https://doi.org/10.1016/j.rser.2022.112166>.
- Deng, B., Zhu, J., Wang, G., Xu, C., Zhang, X., Wang, P., Yuan, Q., 2022. Effects of three major nutrient contents, compost thickness and treatment time on larval weight, process performance and residue component in black soldier fly larvae (*Hermetia illucens*) composting. *J. Environ. Manage.* 307, 14610. <https://doi.org/10.1016/j.jenvman.2022.114610>.
- Du, L., Li, Z., Ding, S., Chen, C., Qu, S., Yi, W., Lu, J., Ding, J., 2019. Synthesis and characterization of carbon-based MgO catalysts for biodiesel production from castor oil. *Fuel* 258, 116122. <https://doi.org/10.1016/j.fuel.2019.116122>.
- Ennaceri, H., Fischer, K., Schulze, A., Moheimani, N.R., 2022. Membrane fouling control for sustainable microalgal biodiesel production: A review. *Renew. Sust. Energ. Rev.* 161, 112335. <https://doi.org/10.1016/j.rser.2022.112335>.
- Fadhil, A.B., Nayyef, A.W., Al-Layla, N.M.T., 2019. Biodiesel production from nonedible feedstock, radish seed oil by cosolvent method at room temperature: evaluation and analysis of biodiesel. *Energ. Source. Part A* 1–11. <https://doi.org/10.1080/15567036.2019.1604902>.
- Falowo, O.A., Betiku, E., 2022. A novel heterogeneous catalyst synthesis from agrowastes mixture and application in transesterification of yellow oleander-rubber oil: Optimization by Taguchi approach. *Fuel* 312, 122999. <https://doi.org/10.1016/j.fuel.2021.122999>.
- Falowo, O.A., Ojumu, T.V., Perea, O., Betiku, E., 2020. Sustainable biodiesel synthesis from honne-rubber-neem oil blend with a novel mesoporous base catalyst synthesized from a mixture of three agrowastes. *Catalysts* 10, 190. <https://doi.org/10.3390/catal10020190>.
- Feng, W.L., Huang, P., Wang, B.C., Wang, C.W., Wang, W.G., Wang, T.L., Chen, S.F., Lv, R.L., Qin, Y.H., Ma, J.Y., 2016. Solvothermal synthesis of ZnO with different morphologies in dimethylacetamide media. *Ceram. Int.* 42, 2250–2256. <https://doi.org/10.1016/j.ceramint.2015.10.018>.
- Feng, W.L., Xiong, H., Wang, W.G., Duan, X.L., Yang, T., Wu, C., Yang, F., Xiong, J., Wang, T.L., Wang, C.W., 2019. Energy consumption analysis of lipid extraction from black soldier fly biomass. *Energy* 185, 1076–1085. <https://doi.org/10.1016/j.energy.2019.07.113>.
- Figueiredo, J.L., Pereira, M.F.R., Freitas, M.M.A., Órfão, J.J.M., 2007. Characterization of active sites on carbon catalysts. *Ind. Eng. Chem. Res.* 46, 4110–4115. <https://doi.org/10.1021/ie061071v>.
- Gohain, M., Laskar, K., Phukon, H., Bora, U., Kalita, D., Deka, D., 2020. Towards sustainable biodiesel and chemical production: Multifunctional use of heterogeneous catalyst from littered *Tectona grandis* leaves. *Waste Manage.* 102, 212–221. <https://doi.org/10.1016/j.wasman.2019.10.049>.
- Guisnet, M., Magnoux, P., 2001. Organic chemistry of coke formation. *Appl. Catal. A: Gen.* 212, 83–96. [https://doi.org/10.1016/S0926-860X\(00\)00845-0](https://doi.org/10.1016/S0926-860X(00)00845-0).
- Guo, H., Jiang, C., Zhang, Z., Lu, W., Wang, H., 2021. Material flow analysis and life cycle assessment of food waste bioconversion by black soldier fly larvae (*Hermetia illucens* L.). *Sci. Total Environ.* 750, 141656. <https://doi.org/10.1016/j.scitotenv.2020.141656>.
- Gurunathan, B., Ravi, A., 2015. Process optimization and kinetics of biodiesel production from neem oil using copper doped zinc oxide heterogeneous nanocatalyst. *Bioresource Technol.* 190, 424–428. <https://doi.org/10.1016/j.biortech.2015.04.101>.
- Hsiao, M.C., Lin, C.C., Chang, Y.H., 2011. Microwave irradiation-assisted transesterification of soybean oil to biodiesel catalyzed by nanopowder calcium oxide. *Fuel* 90, 1963–1967. <https://doi.org/10.1016/j.fuel.2011.01.004>.
- Hwa, S., Goto, M., Taufiqyap, Y.H., 2015. Biodiesel production from *Jatropha curcas* L. oil with Ca and La mixed oxide catalyst in near supercritical methanol conditions. *J. Supercrit. Fluid* 104, 243–250. <https://doi.org/10.1016/j.supflu.2015.06.023>.
- Ibrahim, S.F., Asikin-mijan, N., Ibrahim, M.L., Abdulkareem-alsultan, G., 2020. Sulfonated functionalization of carbon derived corncob residue via hydrothermal synthesis route for esterification of palm fatty acid distillate. *Energ. Convers. Manage.* 210, 112698. <https://doi.org/10.1016/j.enconman.2020.112698>.
- Jeon, H., Kim, D.J., Kim, S.J., Kim, J.H., 2013. Synthesis of mesoporous MgO catalyst templated by a PDMS-PEO comb-like copolymer for biodiesel production. *Fuel Process Technol.* 116, 325–331. <https://doi.org/10.1016/j.fuproc.2013.07.013>.
- Kazmi, J., Ooi, P.C., Goh, B.T., Lee, M.K., Wee, M.F.M.R., Karim, S.S.A., Raza, S.R.A., Mohamed, M.A., 2020. Bi-doping improves the magnetic properties of zinc oxide nanowires. *RSC Adv.* 2020 (10), 23297–23311. <https://doi.org/10.1039/D0RA03816D>.
- Khan, H.M., Iqbal, T., Ali, C.H., Yasin, S., Jamil, F., 2020a. Waste quail beaks as renewable source for synthesizing novel catalysts for biodiesel production. *Renew. Energ.* 154, 1035–1043. <https://doi.org/10.1016/j.renene.2020.03.079>.
- Khan, I.W., Naeem, A., Farooq, M., Mahmood, T., Ahmad, B., Hamayun, M., Ahmad, Z., Saeed, T., 2020b. Catalytic conversion of spent frying oil into biodiesel over raw and 12-tungstophosphoric acid modified clay. *Renew. Energ.* 155, 181–188. <https://doi.org/10.1016/j.renene.2020.03.123>.
- Khan, I.W., Naeem, A., Farooq, M., Ud din, I., Ghazi, Z.A., 2021. Reusable Na-SiO₂@CeO₂ catalyst for efficient biodiesel production from non-edible wild olive oil as a new and potential feedstock. *Energ. Convers. Manage.* 231, 113854. <https://doi.org/10.1016/j.enconman.2021.113854>.
- Kouzu, M., Hidaka, J.S., Komichi, Y., Nakano, H., Yamamoto, M., 2009. A process to transesterify vegetable oil with methanol in the presence of quick lime bit functioning as solid base catalyst. *Fuel* 88, 1983–1990. <https://doi.org/10.1016/j.fuel.2009.03.013>.
- Kwong, T.L., Yung, K.F., 2016. One-step production of biodiesel through simultaneous esterification and transesterification from

- highly acidic unrefined feedstock over efficient and recyclable ZnO nanostar catalyst. *Renew. Energ.* 90, 450–457. <https://doi.org/10.1016/j.renene.2016.01.028>.
- Lalander, C., Diener, S., Zurbrugg, C., Vinneras, B., 2019. Effects of feedstock on larval development and process efficiency in waste treatment with black soldier fly (*Hermetia illucens*). *J. Clean. Prod.* 208, 211–219. <https://doi.org/10.1016/j.jclepro.2018.10.017>.
- Li, Z., Ding, S., Chen, C., Qu, S., Du, L., Lu, J., Ding, J., 2019b. Recyclable Li/NaY zeolite as a heterogeneous alkaline catalyst for biodiesel production: process optimization and kinetics study. *Energ. Convers. Manage.* 192, 335–345. <https://doi.org/10.1016/j.enconman.2019.04.053>.
- Li, W., Li, Q., Zheng, L., Wang, Y., Zhang, J., Yu, Z., Zhang, Y., 2015b. Potential biodiesel and biogas production from corncob by anaerobic fermentation and black soldier fly. *Bioresource Technol.* 194, 276–282. <https://doi.org/10.1016/j.biortech.2015.06.112>.
- Li, H., Niu, S.L., Lu, C.M., Cheng, S.Q., 2015a. Comparative evaluation of thermal degradation for biodiesels derived from various feedstocks through transesterification. *Energ. Convers. Manage.* 98, 81–88. <https://doi.org/10.1016/j.enconman.2015.03.097>.
- Li, H., Liu, F., Ma, X., Wu, Z., Li, Y., Zhang, L., Zhou, S., Helian, Y., 2019a. Catalytic performance of strontium oxide supported by MIL-100(Fe) derivative as transesterification catalyst for biodiesel production. *Energ. Convers. Manage.* 180, 401–410. <https://doi.org/10.1016/j.enconman.2018.11.012>.
- Li, Y., Niu, S., Wang, J., Zhou, W., Wang, Y., Han, K., Lu, C., 2022. Mesoporous SrTiO₃ perovskite as a heterogeneous catalyst for biodiesel production: Experimental and DFT studies. *Renew. Energ.* 184, 164–175. <https://doi.org/10.1016/j.renene.2021.11.078>.
- Liang, D., Alam, M.A., Lu, L., Fan, R., Xu, J., Wu, J., 2022. Water-plasma-enhanced and phase-separation-assisted extraction of microalgal lipid for biodiesel production. *Bioresource Technol.* 354, 127198. <https://doi.org/10.1016/j.biortech.2022.127198>.
- Liu, F., Zhang, Y., 2011. Controllable growth of “multi-level tower” ZnO for biodiesel production. *Ceram. Int.* 37, 3193–3202. <https://doi.org/10.1016/j.ceramint.2011.05.087>.
- Lokhande, C.D., Gondkar, P.M., Mane, R.S., Shinde, V.R., Han, S. H., 2009. CBD grown ZnO-based gas sensors and dye-sensitized solar cells. *J. Alloy. Compd.* 475, 304–311. <https://doi.org/10.1016/j.jallcom.2008.07.025>.
- Macawile, M.C., Quitain, A.T., Kida, T., Tan, R., Aureseni, J., 2020. Green synthesis of sulfonated organosilane functionalized multi-walled carbon nanotubes and its catalytic activity for one-pot conversion of high free fatty acid seed oil to biodiesel. *J. Clean. Prod.* 275, 123146. <https://doi.org/10.1016/j.jclepro.2020.123146>.
- Macina, A., Medeiros, T.V., Naccache, R., 2019. A carbon dot-catalyzed transesterification reaction for the production of biodiesel. *J. Mater. Chem. A* 7, 23794–23802. <https://doi.org/10.1039/c9ta05245c>.
- Malhotra, R., Ali, A., 2019. 5-Na/ZnO doped mesoporous silica as reusable solid catalyst for biodiesel production via transesterification of virgin cottonseed oil. *Renew. Energ.* 133, 606–619. <https://doi.org/10.1016/j.renene.2018.10.055>.
- Mansir, N., Taufiq-yap, Y.H., Rashid, U., Lokman, I.M., 2017a. Investigation of heterogeneous solid acid catalyst performance on low grade feedstocks for biodiesel production : a review. *Energ. Convers. Manage.* 141, 171–182. <https://doi.org/10.1016/j.enconman.2016.07.037>.
- Mansir, N., Teo, S.H., Ibrahim, M.L., Hin, T.Y.Y., 2017b. Synthesis and application of waste egg shell derived CaO supported W-Mo mixed oxide catalysts for FAME production from waste cooking oil: Effect of stoichiometry. *Energ. Convers. Manage.* 151, 216–226. <https://doi.org/10.1016/j.enconman.2017.08.069>.
- Mardiah, H.H., Ong, H.C., Masjuki, H.H., Lim, S., Pang, Y.L., 2017. Investigation of carbon-based solid acid catalyst from *Jatropha curcas* biomass in biodiesel production. *Energ. Convers. Manage.* 144, 10–17. <https://doi.org/10.1016/j.enconman.2017.04.038>.
- Margellou, A., Koutsouki, A., Petrakis, D., Vaimakis, T., Manos, G., Kontominas, M., Pomonis, P., 2018. Enhanced production of biodiesel over MgO catalysts synthesized in the presence of Poly-Vinyl-Alcohol (PVA). *Ind. Crop. Prod.* 114, 146–153. <https://doi.org/10.1016/j.indcrop.2018.01.079>.
- Medeiros, T.V., Macina, A., Naccache, R., 2020. Graphitic carbon nitrides: Efficient heterogeneous catalysts for biodiesel production. *Nano Energy* 78, 105306. <https://doi.org/10.1016/j.nanoen.2020.105306>.
- Moreno-Castilla, C., Carrasco-Marín, F., Parejo-Pérez, C., López Ramón, M.V., 2001. Dehydration of methanol to dimethyl ether catalyzed by oxidized activated carbons with varying surface acidic character. *Carbon* 39, 869–875. [https://doi.org/10.1016/S0008-6223\(00\)00192-5](https://doi.org/10.1016/S0008-6223(00)00192-5).
- Mutreja, V., Singh, S., Ali, A., 2014. Potassium impregnated nanocrystalline mixed oxides of La and Mg as heterogeneous catalysts for transesterification. *Renew. Energ.* 62, 226–233. <https://doi.org/10.1016/j.renene.2013.07.015>.
- Nath, B., Das, B., Kalita, P., Basumatary, S., 2019. Waste to value addition: Utilization of waste Brassica nigraplant derived novel green heterogeneous base catalyst for effective synthesis of biodiesel. *J. Clean. Prod.* 239, 118112. <https://doi.org/10.1016/j.jclepro.2019.118112>.
- Negm, N.A., Sayed, G.H., Yehia, F.Z., Habib, O.I., Mohamed, E.A., 2017. Biodiesel production from one-step heterogeneous catalyzed process of Castor oil and *Jatropha* oil using novel sulphonated phenyl silane montmorillonite catalyst. *J. Mol. Liq.* 234, 157–163. <https://doi.org/10.1016/j.biortech.2012.04.098>.
- Obadiah, A., Swaroopa, G.A., Kumar, S.V., Jeganathan, K.R., Ramasubbu, A., 2012. Biodiesel production from Palm oil using calcined waste animal bone as catalyst. *Bioresource Technol.* 1116, 512–516. <https://doi.org/10.1016/j.biortech.2012.03.112>.
- Pan, H., Liu, Y., Xia, Q., Zhang, H., Guo, L., Li, H., Jiang, L., Yang, S., 2020. Synergetic combination of mesoporous polymeric acid and base enables heterogeneous catalytic one-pot highly efficient conversion of crude *Jatropha* oil into biodiesel. *Green Chem.* 22, 1698–1709. <https://doi.org/10.1039/C9GC04135D>.
- Pathak, G., Das, D., Rajkumari, K., Rokhum, S.L., 2018. Exploiting waste: Towards a sustainable production of biodiesel using *Musa acuminata* peel ash as a heterogeneous catalyst. *Green Chem.* 20, 2365–2373. <https://doi.org/10.1039/c8gc00071a>.
- Pereira, M.F.R., Órfão, J.J.M., Figueiredo, J.L., 1999. Oxidative dehydrogenation of ethylbenzene on activated carbon catalysts. I. Influence of surface chemical groups. *Appl. Catal. A: Gen.* 184, 153–160. [https://doi.org/10.1016/S0926-860X\(99\)00124-6](https://doi.org/10.1016/S0926-860X(99)00124-6).
- Proc, K., Bulak, P., Wiacek, D., Bieganski, A., 2020. *Hermetia illucens* exhibits bioaccumulative potential for 15 different elements-Implications for feed and food production. *Sci. Total Environ.* 723, 138125. <https://doi.org/10.1016/j.scitotenv.2020.138125>.
- Putra, M.D., Irawan, C., Udiantoro, R.Y., Nata, I.F., 2018. A cleaner process for biodiesel production from waste cooking oil using waste materials as a heterogeneous catalyst and its kinetic study. *J. Clean. Prod.* 195, 1249–1258. <https://doi.org/10.1016/j.jclepro.2018.06.010>.
- Qu, S., Chen, C., Guo, M., Jiang, W., Lu, J., Yi, W., Ding, J., 2021. Microwave-assisted in-situ transesterification of *Spirulina platensis* to biodiesel using PEG/MgO/ZSM-5 magnetic catalyst. *J. Clean. Prod.* 311, 127490. <https://doi.org/10.1016/j.jclepro.2021.127490>.
- Raksasat, R., Lim, J.W., Kiatkittipong, W., Kiatkittipong, K., Ho, Y. C., Lam, M.K., Font-Palma, C., Zaid, H.F.M., Cheng, C.K., 2020. A review of organic waste enrichment for inducing palatability of black soldier fly larvae: Wastes to valuable resources. *Environ. Pollut.* 267, 115488. <https://doi.org/10.1016/j.envpol.2020.115488>.

- Rehman, K., Cai, M., Xiao, X., Zheng, L., Wang, H., Soomro, A.A., Zhou, Y., Li, W., Yu, Z., Zhang, J., 2017. Cellulose decomposition and larval biomass production from the co-digestion of dairy manure and chicken manure by mini-livestock (*Hermetia illucens* L.). *J. Environ. Manage.* 196, 458–465. <https://doi.org/10.1016/j.jenvman.2017.03.047>.
- Roy, T., Sahani, S., Madhu, D., Sharma, Y.C., 2020. A clean approach of biodiesel production from waste cooking oil by using single phase BaSnO_3 as solid base catalyst: Mechanism, kinetics & E-study. *J. Clean. Prod.* 265, 121440. <https://doi.org/10.1016/j.jclepro.2020.121440>.
- Sahani, S., Roy, T., Sharma, Y.C., 2019. Clean and efficient production of biodiesel using barium cerate as a heterogeneous catalyst for the biodiesel production; kinetics and thermodynamic study. *J. Clean. Prod.* 237, 117699. <https://doi.org/10.1016/j.jclepro.2019.117699>.
- Sangar, S.K., Syazwani, O.N., Farabi, M.S.A., Razali, S.M., Shobhana, G., Teo, S.H., Taufiq-Yap, Y.H., 2019. Effective biodiesel synthesis from palm fatty acid distillate (PFAD) using carbon-based solid acid catalyst derived glycerol. *Renew. Energ.* 142, 658–667. <https://doi.org/10.1016/j.renene.2019.04.118>.
- Santana, A., Maçaira, J., Larrayoz, M.A., 2012. Continuous production of biodiesel using supercritical fluids: A comparative study between methanol and ethanol. *Fuel Process Technol.* 102, 110–115. <https://doi.org/10.1016/j.fuproc.2012.04.014>.
- Saravanan, K., Tyagi, B., Shukla, R.S., Bajaj, H.C., 2015. Esterification of palmitic acid with methanol over template-assisted mesoporous sulfated zirconia solid acid catalyst. *Appl. Catal. B-Environ.* 172–173, 108–115. <https://doi.org/10.1016/j.apcatb.2015.02.014>.
- Singh, V., Bux, F., Sharma, Y.C., 2016. A low cost one pot synthesis of biodiesel from waste frying oil (WFO) using a novel material, b-potassium dizirconate ($\text{b-K}_2\text{Zr}_2\text{O}_5$). *Appl. Energ.* 172, 23–33. <https://doi.org/10.1016/j.apenergy.2016.02.135>.
- Soltani, S., Khanian, N., Choong, T.S.Y., Asim, N., Zhao, Y., 2021. Microwave-assisted hydrothermal synthesis of sulfonated TiO_2 -GO core-shell solid spheres as heterogeneous esterification mesoporous catalyst for biodiesel production. *Energ. Convers. Manage.* 238, 114165. <https://doi.org/10.1016/j.enconman.2021.114165>.
- Song, W., Zhang, Y., Varyambath, A., Kim, J.S., Kim, I., 2020. Sulfonic acid modified hollow polymer nanospheres with tunable wall-thickness for improving biodiesel synthesis efficiency. *Green Chem.* 22, 3572–3583. <https://doi.org/10.1039/D0GC00905A>.
- Tang, Z.E., Lim, S., Pang, Y.L., Shuit, S.H., Ong, H.C., 2020. Utilisation of biomass wastes based activated carbon supported heterogeneous acid catalyst for biodiesel production. *Renew. Energ.* 158, 91–102. <https://doi.org/10.1016/j.renene.2020.05.119>.
- Tantirungrotechai, J., Thepatee, S., Yoosuk, B., 2013. Biodiesel synthesis over Sr/MgO solid base catalyst. *Fuel* 106, 279–284. <https://doi.org/10.1016/j.fuel.2013.01.028>.
- Tsanaktsidis, C.G., Christidis, S.G., Favvas, E.P., 2013. A novel method for improving the physicochemical properties of diesel and jet fuel using polyaspartate polymer additives. *Fuel* 104, 155–162. <https://doi.org/10.1016/j.fuel.2012.09.076>.
- Viola, E., Blasi, A., Valerio, V., Guidi, I., Zimbardi, F., Braccio, G., Giordano, G., 2012. Biodiesel from fried vegetable oils via transesterification by heterogeneous catalysis. *Catal. Today* 179, 185–190. <https://doi.org/10.1016/j.cattod.2011.08.050>.
- Wang, Y.T., Fang, Z., Zhang, F., 2018. Esterification of oleic acid to biodiesel catalyzed by a highly acidic carbonaceous catalyst. *Catal. Today* 319, 172–181. <https://doi.org/10.1016/j.cattod.2018.06.041>.
- Yusuff, A.S., Bhonsle, A.K., Trivedi, J., Bangwal, D.P., Singh, L.P., Atray, N., 2021. Synthesis and characterization of coal fly ash supported zinc oxide catalyst for biodiesel production using used cooking oil as feed. *Renew. Energ.* 170, 302–314. <https://doi.org/10.1016/j.renene.2021.01.101>.
- Zhang, X.L., Qiao, R., Qiu, R., Kim, J.C., Kang, K.S., 2009. Fabrication of hierarchical ZnO nanostructures via a surfactant-directed process. *Cryst. Growth Des.* 9, 2906–2910. <https://doi.org/10.1021/cg900226h>.
- Zhao, J., Yang, L., Li, F., Yu, R., Jin, C., 2009. Structural evolution in the graphitization process of activated carbon by high-pressure sintering. *Carbon* 47, 744–751. <https://doi.org/10.1016/j.carbon.2008.11.006>.
- Zhao, C., Yang, L., Xing, S., Luo, W., Wang, Z., Lv, P., 2018. Biodiesel production by a highly effective renewable catalyst from pyrolytic rice husk. *J. Clean. Prod.* 199, 772–780. <https://doi.org/10.1016/j.jclepro.2018.07.242>.
- Zheng, L., Li, Q., Zhang, J., Yu, Z., 2012. Double the biodiesel yield: Rearing black soldier fly larvae, *Hermetia illucens*, on solid residual fraction of restaurant waste after grease extraction for biodiesel production. *Renew. Energ.* 41, 75–79. <https://doi.org/10.1016/j.renene.2011.10.004>.
- Zong, M.H., Duan, Z.Q., Lou, W.Y., Smith, T.J., Wu, H., 2007. Preparation of a sugar catalyst and its use for highly efficient production of biodiesel. *Green Chem.* 9, 434–437. <https://doi.org/10.1039/B615447F>.